Nuclear Inst. and Methods in Physics Research, A 919 (2019) 16–26

Contents lists available at ScienceDirect

Nuclear Inst. and Methods in Physics Research, A

journal homepage: www.elsevier.com/locate/nima

Radiation resistant LGAD design

M. Ferrero [a], R. Arcidiacono [a,b], M. Barozzi [c,e], M. Boscardin [c,e], N. Cartiglia [a,*], G.F. Dalla Betta [d,e], Z. Galloway [g], M. Mandurrino [a], S. Mazza [g], G. Paternoster [c,e], F. Ficorella [c,e], L. Pancheri [d,e], H-F W. Sadrozinski [g], F. Siviero [a,f], V. Sola [a,f], A. Staiano [a], A. Seiden [g], M. Tornago [a,f], Y. Zhao [g]

[a] INFN, Torino, Italy
[b] Università del Piemonte Orientale, Italy
[c] Fondazione Bruno Kessler, Trento, Italy
[d] Università di Trento, Trento, Italy
[e] TIFPA-INFN, via Sommarive 18, 38123, Povo (TN), Italy
[f] Università di Torino, Torino, Italy
[g] SCIPP, University of California Santa Cruz, CA, USA

ARTICLE INFO

Keywords:
Silicon
Timing
LGAD
Acceptor removal

ABSTRACT

In this paper, we report on the radiation resistance of 50-micron thick Low Gain Avalanche Diodes (LGAD) manufactured at the Fondazione Bruno Kessler (FBK) employing different dopings in the gain layer. LGADs with a gain layer made of Boron, Boron low-diffusion, Gallium, Carbonated Boron and Carbonated Gallium have been designed and successfully produced at FBK. These sensors have been exposed to neutron fluences up to $\phi_n \sim 3 \cdot 10^{16}\ n/cm^2$ and to proton fluences up to $\phi_p \sim 9 \cdot 10^{15}\ p/cm^2$ to test their radiation resistance. The experimental results show that Gallium-doped LGAD are more heavily affected by the initial acceptor removal mechanism than those doped with Boron, while the addition of Carbon reduces this effect both for Gallium and Boron doping. The Boron low-diffusion gain layer shows a higher radiation resistance than that of standard Boron implant, indicating a dependence of the initial acceptor removal mechanism upon the implant density.

The LGAD design evolves the standard silicon sensors design by incorporating low, controlled gain [1] in the signal formation mechanism. The overarching idea is to manufacture silicon detectors with signals large enough to assure excellent timing performance while maintaining almost unchanged levels of noise [2].

Charge multiplication in silicon sensors happens when the charge carriers (electrons and holes) are in electric fields of the order of $E \sim 300$ kV/cm [3]. Under this condition, the electrons (and to less extent the holes) acquire sufficient kinetic energy to generate additional e/h pairs by impact ionization. Field values of ~300 kV/cm can be obtained by implanting an appropriate acceptor (or donor) charge density ρ_A (of the order $\rho_A \sim 10^{16}/\mathrm{cm}^3$) that, when depleted, locally generates very high fields. For this reason, an additional doping layer has been added at the $n-p$ junction in the LGAD design, Fig. 1.

1. Initial acceptor removal in LGAD sensors

It has been shown in previous studies [4,5] that neutrons and charged hadrons irradiations reduce the value of gain in LGADs. This effect is due to the *initial acceptor removal* mechanism that progressively deactivates the acceptors forming the gain layer. The effects of initial acceptor removal on the silicon sensor bulk has been first measured in standard Boron-doped silicon sensors more than 20 years ago [6]. Concurrently with the initial acceptor removal mechanism, irradiation causes also the creation of acceptor-like defects due to the creation of deep traps. The combined effects are described by Eq. (1) [2,7]

$$\rho_A(\phi) = g_{eff}\phi + \rho_A(0)e^{-c\phi}, \tag{1}$$

where $g_{eff} = 0.02$ [cm^{-1}] (see for example chapter 5 of [8]), ϕ the irradiation fluence [cm^{-2}], $\rho_A(0)$ ($\rho_A(\phi)$) the initial (after a fluence ϕ) acceptor density [cm^{-3}], and c [cm^2] is a constant that depends on the initial acceptor concentration $\rho_A(0)$ and on the type of irradiation. The first term of Eq. (1) accounts for acceptor creation by deep traps while the second term for the initial acceptor removal mechanism. The factor c can be rewritten as $\phi_o = 1/c$, making more apparent its meaning: ϕ_o is the fluence needed to reduce the initial doping density $\rho_A(0)$ to 1/e of its initial value.

The microscopic origin of the acceptor removal mechanism has not been fully understood, however, it is plausible that the progressive inactivation of the Boron atoms with irradiation happens via the formation of ion-acceptor complexes. In this model, the active (substitutionals) doping elements are removed from their lattice sites due to a 2-step process: (i) the radiation produces interstitial Si atoms that subsequently

* Corresponding author.
E-mail address: cartiglia@to.infn.it (N. Cartiglia).

https://doi.org/10.1016/j.nima.2018.11.121
Received 6 February 2018; Received in revised form 20 November 2018; Accepted 26 November 2018
Available online 30 November 2018

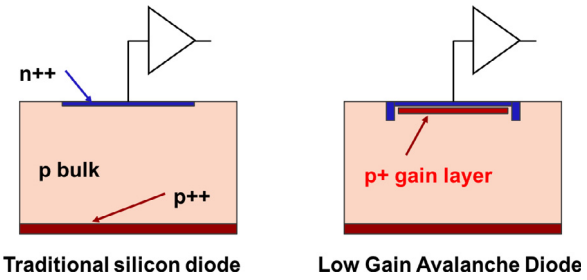

Fig. 1. Schematic of a traditional silicon diode (left) and of a Low-Gain Avalanche Diode (right). The additional p^+ layer underneath the n^{++} electrode creates, when depleted, a large electric field that generates charge multiplications.

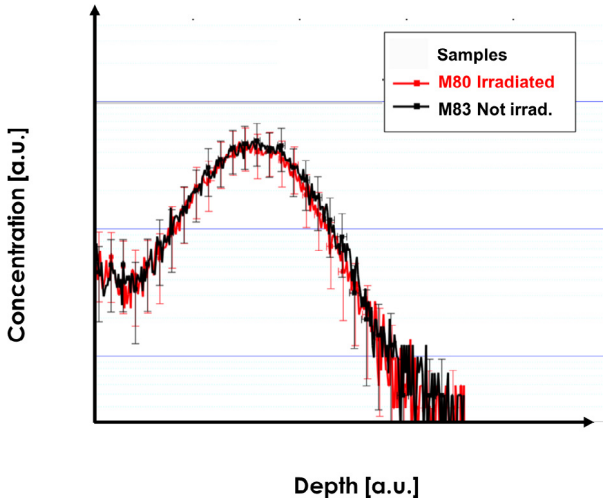

Fig. 2. Density of Boron atoms forming the gain layer in a new (M83) and a heavily irradiated (M80, irradiated to $1 \cdot 10^{16}$ n_{eq}/cm^2) LGAD. Even though the gain layer of the M80 sensor is almost completely deactivated, M83 and M80 have the same gain layer doping profile (the plot has log-y and lin-x axis).

(ii) inactivate the doping elements via kick-out reactions (Watkins mechanism [9]) that produce ion-acceptor complexes (interstitials) [10].

Secondary Ion Mass Spectrometer (SIMS) measurements support this view: Fig. 2 shows the densities of Boron atoms forming the gain layer as a function of depth in a new (M83) and a heavily irradiated (M80, irradiated to $\phi \sim 1 \cdot 10^{16}$ n_{eq}/cm^2) LGAD where the gain layer has completely disappeared. Remarkably, the SIMS results are almost identical: the decrease of the active gain layer doping in irradiated sensors does not correspond to a disappearance of the Boron atoms, only to their inactivation. The SIMS were performed in the central area of 1 mm^2 LGADs

1.1. A parametrization of the acceptor removal mechanism

In a simple model of acceptor removal, the density of initial acceptor atoms deactivated by radiation is given by the product of the fluence ϕ_o times the silicon atomic density ρ_{Si} times the cross section for an impinging particle to deactivate an acceptor σ_{Acc}:

$$(1 - 1/e)\rho_A(0) = \phi_o \cdot \rho_{Si} \cdot \sigma_{Acc}, \quad (2)$$

$$\rho_A(0) = \frac{1}{0.63}\phi_o \cdot \rho_{Si} \cdot \sigma_{Acc}, \quad (3)$$

where $\rho_{Si} = 5 \cdot 10^{22}$ cm^{-3}. Following the two-step model outlined above, the expression of σ_{Acc} can be written as the product of the cross section between radiation and Silicon (σ_{Si}) times the number of interstitials generated in the scattering (N_{Int}) times the probability of capturing an

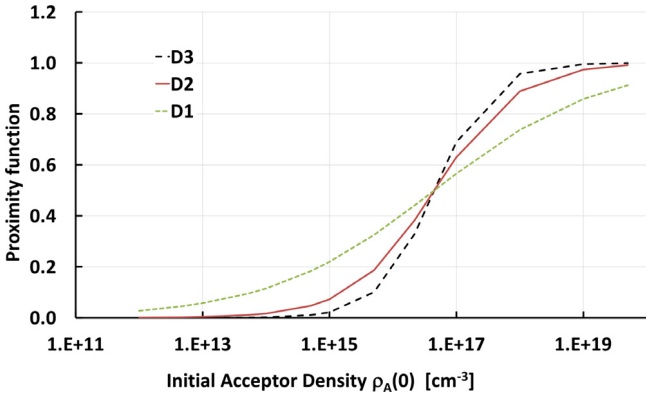

Fig. 3. Proximity functions D1, D2, and D3. The value $\rho_{Ao} = 2.5 \cdot 10^{16}$ n/cm^3 has been used in this plot.

acceptor (k_{cap}):

$$\sigma_{Acc} = k_{cap} \cdot N_{Int} \cdot \sigma_{Si}. \quad (4)$$

Note that the presence of impurities (Carbon, Oxygen, ...) influence the value of k_{cap} as they might intercept the interstitial atoms before they reach the acceptors.

Eq. (2) assumes that each interstitial atom created by radiation is in the proximity of acceptors, however this might not be the case at low acceptor density. For this reason, a proximity function D needs to be included in Eq. (2): this function describes the probability that an interstitial atom is in the vicinity of an acceptor atom. The analytic form of D is not unique, any smooth function that goes to 0 at low acceptor density and to 1 at large density is acceptable, for example:

$$Dn = \frac{1}{1 + (\frac{\rho_{Ao}}{\rho_A(0)})^{n/3}}, \quad (5)$$

where ρ_{Ao} is a fit parameter indicating the acceptor density at which an interstitial state has a probability of 0.5 of being in the vicinity of an acceptor and n is an exponent that needs to be determined experimentally. Fig. 3 shows the values of D1, D2 and D3 (n = 1, 2 or 3) with $\rho_{Ao} = 2.5 \cdot 10^{16}$ n/cm^3.

Combining Eqs. (2) and (5), the expression linking the fluence ϕ_o to the number of deactivated acceptors is:

$$\phi_o \cdot \rho_{Si} \cdot \sigma_{Acc} \frac{1}{1 + (\frac{\rho_{Ao}}{\rho_A(0)})^{n/3}} = 0.63\rho_A(0), \quad (6)$$

$$\phi_o = 0.63\frac{\rho_A(0)}{\rho_{Si} \cdot \sigma_{Acc}}(1 + (\frac{\rho_{Ao}}{\rho_A(0)})^{n/3}), \quad (7)$$

where σ_{Acc} and ρ_{Ao} are fit parameters. Analytic expressions of Dn using a linear (D1), a surface (D2) and a volumetric (D3) proximity function were tried, finding the best agreement between models and data with n = 2, σ_{Acc} = 76 mb , and $\rho_{Ao} = 2.5 \cdot 10^{16}$ n/cm^3. The n = 2 result indicates that the clusters have a cylindrical shape since spherical shape would have yield to n = 3. Using these numbers, the parameterizations of Eq. (6) without the proximity function and with each of the three functions (D1, D2, and D3) are superposed in Fig. 4 to experimental points. The experimental points of B-neutrons (Boron gain layer irradiated with reactor neutrons) are taken from [11–13], the B-protons (Boron gain layer irradiated with 800 MeV/c protons) from [11,13] while Ga-neutrons (Gallium gain layer irradiated with reactor neutrons) from [14,15].

The effect of the proximity function is important at low initial acceptor density, where the overlap probability between interstitial states and acceptors is small and therefore a higher fluence is needed to have initial acceptor removal. It is important to stress that the acceptor removal rate might differ upon the irradiation type (pions, protons, neutrons), the irradiation energy, and the acceptor element (Boron or

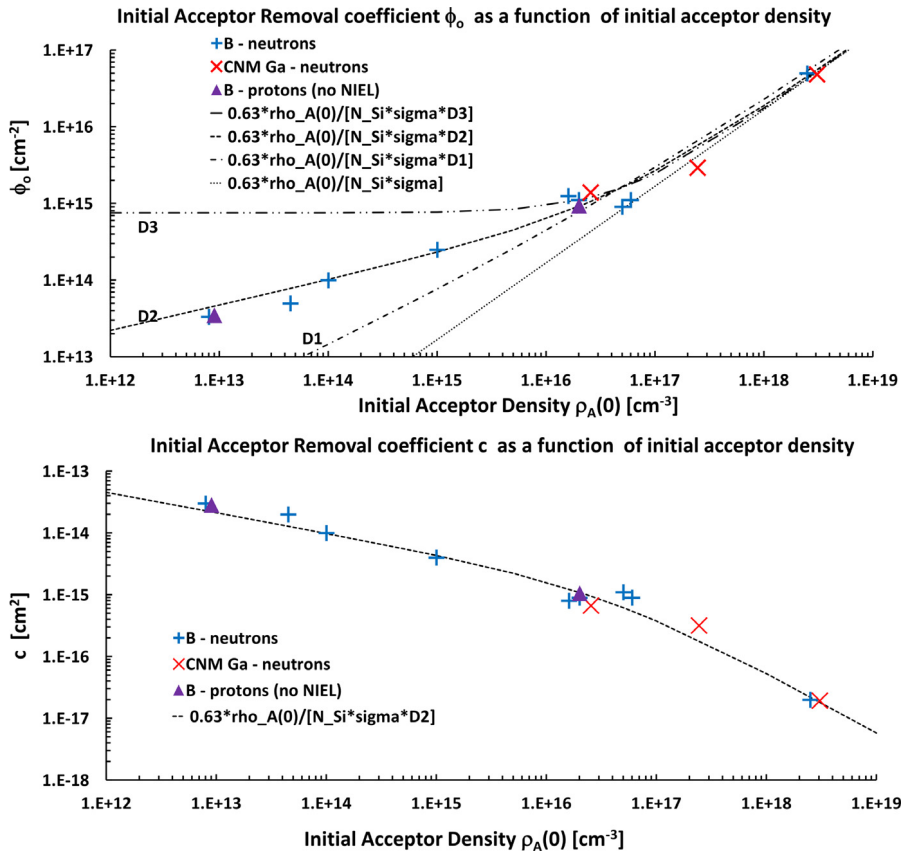

Fig. 4. The two plots show the parametrization of c (bottom) and ϕ_o (top) from Eq. (6) together with experimental points as a function of the initial acceptor density. The top plot also shows the parametrization of Eq. (6) with and without the effect of the proximity functions. The best agreement data-parametrization is obtained with the D2 proximity function.

Gallium), however, for lack of statistics, Fig. 4 shows a single common fit.

Using the D2 parametrization, the absolute and relative effect of radiation on the initial acceptor density can be studied. The left plot of Fig. 5 reports the number of removed acceptors per incident particle per cm^3 as a function of $\rho_A(0)$: it varies from 1 [cm^{-3}] at $\rho_A(0) = 10^{13}$ [cm^{-3}] to $\sim$ 60 [cm^{-3}] at $\rho_A(0) = 10^{19}$ [cm^{-3}]. Even though the number of removed acceptors increases with $\rho_A(0)$, the fraction of removed acceptor is strongly decreasing as a function of $\rho_A(0)$ (Fig. 5, right plot) demonstrating that high initial acceptor densities are less affected by radiation.

From the asymptotic behavior of the left plot of Fig. 5 we can measure the product $N_{Int} * k_{cap}$ and, combining this value with the value of $\sigma_{Acc} = 76$ mb , we can calculate σ_{Si}:

$$k_{cap} \cdot N_{Int} \sim 60, \tag{8}$$

$$\sigma_{Si} = \frac{\sigma_{Acc}}{k_{cap} \cdot N_{Int}} \sim 1.3 \text{ mb}. \tag{9}$$

Both numbers are consistent with the results shown in [16] for 1 MeV neutron on Silicon: $\sigma_{Si} \sim 4$ mb and $N_{Int} \sim 200 - 300$.

Finally, using the terms described above, the expression of the c coefficient can be written as:

$$c = k_{cap} \cdot \frac{\rho_{Si} \cdot N_{Int} \cdot \sigma_{Si}}{0.63\rho_A(0)} \frac{1}{1 + (\frac{\rho_{Ao}}{\rho_A(0)})^{2/3}}, \tag{10}$$

where the capture coefficient k_{cap} depends upon the doping used for the gain layer and the presence of additional impurities such as Carbon or Oxygen.

Acceptor creation and initial acceptor removal mechanisms described by Eq. (1) happen concurrently in the multiplication layer as well as in the bulk. The evolutions of several initial doping densities as a function of neutron fluence are shown schematically in Fig. 6: the initial Boron doping is removed as the fluence increases and in the meantime new acceptor-like states are created. At sufficiently high values of fluence, all initial doping values converge on the doping density of the high resistivity PiN diodes, indicating a complete disappearance of the initial acceptor density.

2. Production of LGAD with different gain layer doping

Three hypotheses have been put forward for the design of more radiation hard LGADs: (i) it has been reported in [15,17] that Gallium might be less prone than Boron to the Watkins mechanism, (ii) the presence of Carbon atoms might slow down the acceptor removal mechanism by producing ion-carbon complexes instead of ion-acceptor complexes, and (iii) a narrower doping layer with higher initial doping should be less prone to the acceptor removal mechanism than a wider doping layer with a lower initial doping.

To test these hypotheses, 50-μm thick LGAD sensors with 5 different gain layer configurations have been manufactured at the Fondazione Bruno Kessler[1] : (i) Boron (B), (ii) Boron low-diffusion (B LD), (iii) Gallium (Ga), (iv) carbonated Boron (B+C), and (v) carbonated Gallium (Ga+C). This production is called *UFSD2*. It is important to note that carbon enrichment has been done uniquely in the volume of the gain layer to avoid a sharp increase of the leakage current. Details on the production have been presented in [18], a short summary of the UFSD2 production is shown in Table 1: 18 6-inch wafers were processed, 10 with a B-doped and 8 with a Ga-doped gain layer. The B-doped gain layer wafers W3–10 have 3 splits dose, in 2% steps, while the Ga-doped gain layer wafers W11–19 have also 3 splits of dose, however in 4% steps. Two splits of B-doped and one of the Ga-doped gain layers have been co-implanted with Carbon, with two different doses of Carbon. Two wafers

[1] FBK, Fondazione Bruno Kessler, Trento, Italy.

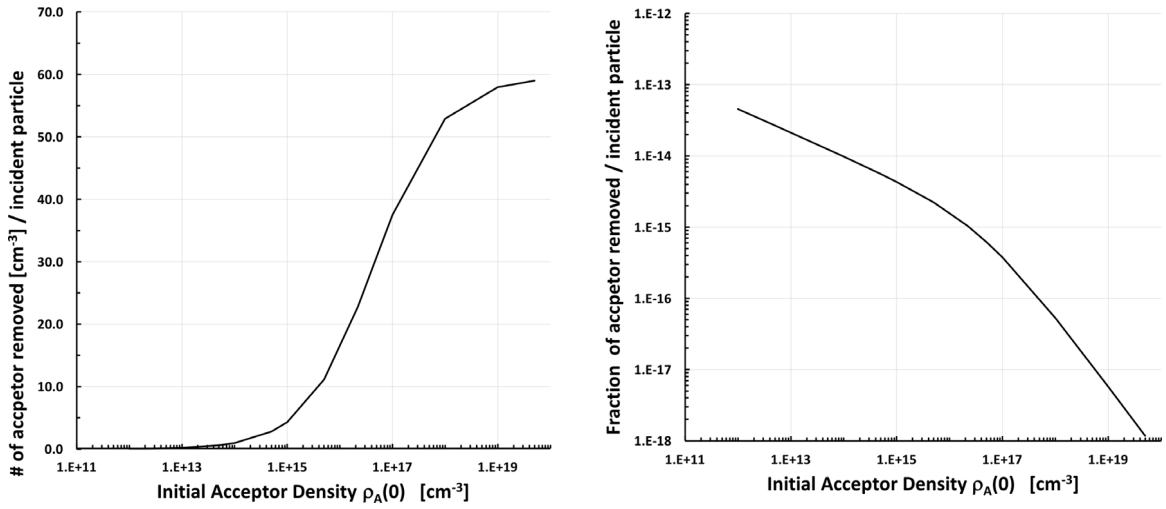

Fig. 5. The left plot shows the number of removed acceptor atoms per cm^3 per incident particle: at the highest acceptor density ~ 60 acceptors/cm^3 are removed per incident particle. The right plot shows instead the fraction of acceptors removed per incident particle demonstrating that the importance of the acceptor removal mechanism is larger at low $\rho_A(0)$ values.

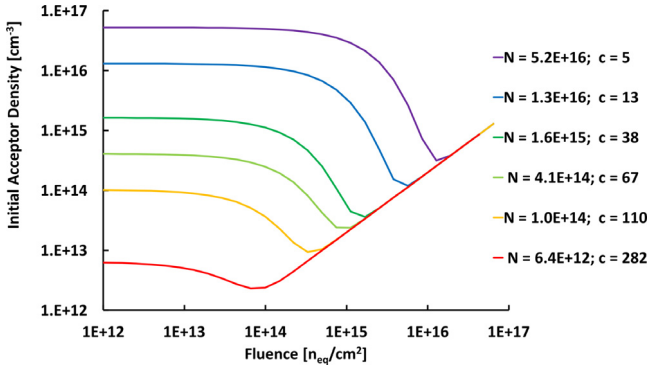

Fig. 6. Evolution of acceptor density as a function of neutron fluence for different initial acceptor densities. The lowest acceptor concentration, $\rho_A = 6 \cdot 10^{12}$ N/cm^3, corresponds to the bulk of a high resistivity PiN sensor. The curves have been obtained with a value of $g_{eff} = 0.02$. The legend reports for each curve the initial acceptor density (in unit of [N/cm^3]) and the value of c (indicated in the legend in unit of [10^{-16} cm^2]) as obtained from the parametrization D2 shown in Fig. 4.

Table 1
Summary of the doping splits in the UFSD2 production. The last column reports the irradiation campaign (p = protons, n = neutrons).

Wafer #	Dopant	Gain dose	Carbon	Diffusion	irradiation
1	Boron	0.98		Low	n
2	Boron	1.00		Low	
3	Boron	1.00		High	p
4	Boron	1.00	Low	High	
5	Boron	1.00	High	High	
6	Boron	1.02	Low	High	p, n
7	Boron	1.02	High	High	
8	Boron	1.02		High	n
9	Boron	1.02		High	
10	Boron	1.04		High	
11	Gallium	1.00		Low	
12	Gallium	1.00		Low	
13	Gallium	1.04		Low	
14	Gallium	1.04		Low	p, n
15	Gallium	1.04	Low	Low	p, n
16	Gallium	1.04	High	Low	
17	Gallium	1.08		Low	
18	Gallium	1.08		Low	

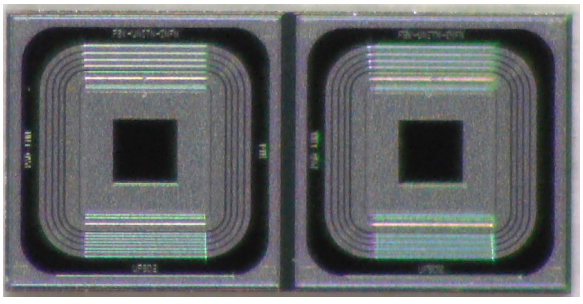

Fig. 7. Example of a pair PiN-LGAD with 4 guard-rings manufactured by FBK used in the analysis presented in this work. Each sensor is 1 × 1 mm^2 and 50-μm thick.

with a B-doped gain layer (W1, 2) were exposed to a reduced thermal load during production to minimize the diffusion of Boron (Boron low-diffusion). The Ga-doped wafers, given the higher diffusivity of Gallium, were also exposed to a reduced thermal load, however, the width of the resulting Gallium implant is nevertheless wider even than that of the B-doped gain layer with a high thermal load.

UFSD2 layout comprises of many hundreds of devices, from 1×1 mm^2 single diodes to large arrays of pads and strips [18]. For this irradiation campaign, pairs of 1 × 1 mm^2 PiN-LGAD diodes were used, as shown in Fig. 7. Combined PiN-LGAD irradiation is a very useful tool in assessing the evolution of the LGAD behavior with fluence, as at each irradiation step the PiN diodes are used as a reference.

2.1. Properties of LGAD with different gain layer doping

Fig. 8 shows on the top pane representative 1/C^2-V curves for B and B+C doped gain layers LGADs while on the bottom those of Ga and Ga+C doped gain layers. The voltage necessary to deplete the gain layer, V_{GL}, is proportional to the average active doping ρ_A in the gain layer:

$$V_{GL} = \frac{q\rho_A}{2\epsilon} w^2 \tag{11}$$

where w is the thickness of the gain layer, normally ~ 1 μm, and q the electron electric charge. Assuming a constant value of w, V_{GL} is directly proportional to ρ_A. In the $1/C^2$-V curves, V_{GL} can be recognized as the point where the 1/C^2-V curve starts a sharp increase, while the voltage of the diode full depletion, V_{FD}, is where the 1/C^2 becomes constant. The voltage difference between V_{FD} and V_{GL}, $\Delta V_{Bulk} = V_{FD} - V_{GL}$, is proportional to the doping of the sensor bulk. For non irradiated sensors, as those shown in Fig. 8, ΔV_{Bulk} is of the order of a few volts indicating a doping of $\rho_{Bulk} \sim 2 - 3 \cdot 10^{12}$ atoms/cm^3. We indicate V_{GL} measured with the $1/C^2$-V curves with the symbol V_{GL}^C.

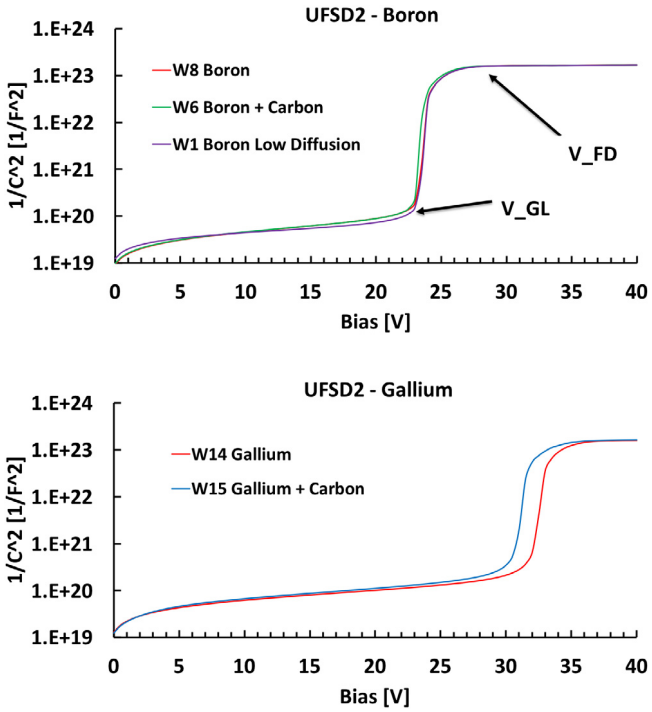

Fig. 8. Average $1/C^2$-V curves for each of the wafer used in the irradiation campaign. The labels on the left plot indicate the points where the gain layer and the bulk deplete. Each curve is the average of 40 diodes.

Table 2
Gain layer FWHM of the wafers used in the irradiation campaign.

Wafer #	Dopant	Gain dose	Width [a.u.]
1	B LD	0.98	1
3	B	1.00	1.3
6	B + C	1.02	1.3
8	B	1.02	1.3
14	Ga	1.04	2.0
15	Ga + C	1.04	1.7

Table 3
Wafers and fluences used in the irradiation campaign.

Wafer #	Dopant	Gain dose	n fluence [10^{15} n_{eq}/cm^2]	p fluence [10^{15} p/cm^2]
1	B LD	0.98	0.2, 0.4, 0.8, 1.5, 3.0, 6.0	
3	B	1.00		0.2, 0.9, 3.9
6	B + C	1.02	0.2, 0.4, 0.8, 1.5, 3.0, 6.0	0.9, 3.9
8	B	1.02	0.2, 0.4, 0.8, 1.5, 3.0, 6.0	
14	Ga	1.04	0.2, 0.4, 0.8, 1.5, 3.0, 6.0	0.9, 3.9
15	Ga + C	1.04	0.2, 0.4, 0.8, 1.5, 3.0, 6.0	0.9, 3.9

It is visible in the plot that Carbon implantation reduces the activated fraction of Gallium, while the Carbon effects on Boron is minimal: V_{GL} is on average 0.3 V smaller for B+C LGADs with respect to that of B LGADs. A discussion of the effects of Carbon co-implantation can be found in [19].

The measurements were taken with the Keysight B1505A parameter analyzer using as the model of the silicon detector a $C_p - R_p$ circuit. The $1/C^2$-V curves were obtained at room temperature with a probing frequency of 1 kHz. The value of the frequency was varied between 1 and 3 kHz finding no dependence of the results on the operating frequency. Analyzing how R_p changes with bias, we noticed that in coincidence with V_{GL}^C the R_p curve presents a sharp decrease, allowing for an easy identification of the exact voltage of the gain layer depletion. We indicate V_{GL} measured with the R_P-V curves with the symbol V_{GL}^R. The correspondence between V_{GL}^C and V_{GL}^R is shown in Fig. 9 for a sensor from W1 irradiated to $3{\cdot}10^{15}$ n_{eq}/cm^2.

In the following analysis, the gain layer depletion voltage has been determined using a combination of the V_{GL}^C and V_{GL}^R values: at low fluences both V_{GL}^C and V_{GL}^R are easily identifiable, while for fluences above $1{\cdot}10^{15}$ n_{eq}/cm^2 the position of V_{GL}^R is easier to identify. The combination of V_{GL}^C and V_{GL}^R allows determining V_{GL} with an uncertainty of 0.5 V.

An interesting parameter to understand the acceptor removal mechanism is the spatial extension of the gain layer. Table 2 reports, in arbitrary unit, the measured FWHM of the gain layer implants for the wafers exposed to irradiation. The implant widths have been extracted from the doping profiles obtained from the $1/C^2$-V curves using the relationship:

$$N(w) = \frac{2}{q\epsilon A^2}\frac{1}{d(1/C(V)^2)/dV} \quad w = \frac{\epsilon A^2}{C(V)}, \tag{12}$$

where $N(w)$ is the doping density at a depth w and A is the diode's area.

These widths are consistent with the observation reported in [19] that carbon co-implantation might yield to narrower implant widths.

3. Irradiation campaign

Table 3 reports the wafers and the irradiation steps used in the irradiation campaign. A set of LGADs was irradiated without bias with neutrons in the JSI research reactor of TRIGA type in Ljubljana. The neutron spectrum and flux are well known [20] and the fluence is quoted in 1 MeV equivalent neutrons per cm^2 (n_{eq}/cm^2). A different set of LGADs was irradiated with protons at the IRRAD CERN irradiation facility [21]. The IRRAD proton facility is located on the T8 beamline at the CERN PS East Hall where the primary proton beam with a momentum of 24 GeV/c is extracted from the PS ring. In IRRAD, irradiation experiments are performed using the primary protons, prior reaching the beam dump located downstream of the T8 beam line. After irradiation, the devices were annealed for 80 min at 60 °C. Afterward, the devices were kept in cold storage at −20 °C. The table reports the actual number of protons: the fluences in n_{eq}/cm^2 can be obtained by multiplying the proton fluences by the NIEL factor (NIEL = 0.6).

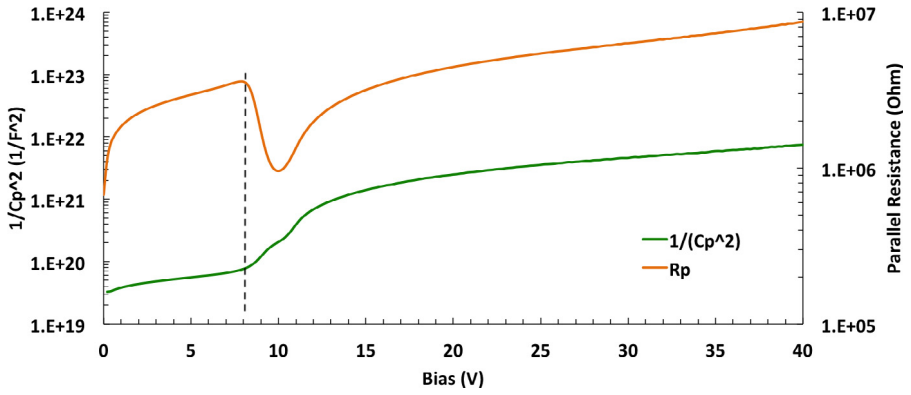

Fig. 9. This plot shows the correspondence between V_{GL}^{C} and V_{GL}^{R} for a sensor from W1 irradiated to $3{\cdot}10^{15}$ n_{eq}/cm^2.

Table 4
Compilation of the initial acceptor removal coefficient for neutrons c_n and protons c_p irradiation for an initial doping density of $\rho(0) \sim 1-2\cdot 10^{16}$ atoms/cm^3. The third column shows the ratio c_n/c_p. The error on the c_n has been estimated to be ± 1.0 while on c_p is ± 1.5. The fourth and fifth columns report the c_p values when the NIEL factor has been applied to the proton fluence.

Gain Layer	c_n [10^{-16} cm^2]	c_p [10^{-16} cm^2] No NIEL	c_n/c_p No NIEL	c_p [10^{-16} cm^2] NIEL	c_n/c_p NIEL
Ga	7.1 ± 1.0	9. ± 1.5	0.79 ± 0.22	15. ± 1.5	0.47 ± 0.08
B	5.4 ± 1.0	6.5 ± 1.5	0.83 ± 0.29	10.8 ± 1.5	0.50 ± 0.11
B LD	4.7 ± 1.0				
Ga + C	4.0 ± 1.0	4.2 ± 1.5	0.95 ± 0.43	7.0 ± 1.5	0.57 ± 0.19
B + C	2.1 ± 1.0	3.3 ± 1.5	0.63 ± 0.66	5.5 ± 1.5	0.38 ± 0.54

4. Simulation of different initial acceptor removal rate

As reported in Eq. (1), the initial acceptor removal effect is parametrized by the function $c(\rho_A(0))$. Using the simulation program WF2[2] [22], the effect of larger or smaller values of c on the reduction of the gain has been simulated. Fig. 10 reports the bias voltage needed to keep a constant gain value = 10 as a function of neutron fluence for the situation where the value of $c(\rho_A(0))$ is twice, a half or a quarter of the presently measured value of $c(\rho_A(0)) = 2-3\cdot 10^{-16}$ cm^{-3} $\sim 6\cdot 10^{-16}$ cm^2. The simulation has been calculated using the parametrization shown in Eq. (1), with $g_{eff} = 0.02\,\mathrm{cm}^{-1}$ and the c values (in unit of [10^{-16} cm^2]) shown in the legend. On the plot, the measured points from Hamamatsu LGADs are also reported [5].

As Fig. 10 shows, when the gain layer doping is progressively deactivated by irradiation, the bias voltage should be increased to compensate for the reduction of the electric field generated by the gain layer. Smaller values of c move the need to increase the bias voltage to progressively higher fluences, making LGAD operation more stable.

5. Results

Fig. 11 shows the evolution of the foot position (V_{GL}^{C}) with increasing neutrons irradiation. The lowest irradiation level is $\phi = 2\cdot 10^{14}$ n_{eq}/cm^2, and the fluence increases by a factor of 2 in each of the following curves.

These plots show clearly that the decrease of V_{GL}^{C} as a function of irradiation for carbonated gain layers is smaller than that of non-carbonated gain layers: for equal fluence, carbonated gain layers retain a higher active doping. Comparing the 4 plots in Fig. 11, it is evident that the slopes of the $1/C^2$ curves at equal fluence are similar, indicating, via equation (12), that the doping of the bulk is evolving in the same way for all sensors.

The $c(\rho_A(0))$ coefficient can be measured by fitting an exponential function to the fraction of still active gain layer as a function of fluence, as shown in Eq. (13):

$$\frac{V_{GL}(\phi)}{V_{GL}(0)} = \frac{\rho_A(\phi)}{\rho_A(0)} = e^{-c(\rho_A(0))\phi}. \tag{13}$$

[2] Shareware at http://cern.ch/nicolo.

Table 5
Compilation of the initial acceptor removal coefficient ϕ_o for neutrons and protons irradiations. As explained in the text, ϕ_o represents the flux needed to remove 63% of the initial acceptors.

Gain Layer	ϕ_o^n [10^{16} cm^{-2}] neutrons irrad.	ϕ_o^p [10^{16} cm^{-2}] protons irrad.
Ga	0.14 ± 0.02	0.11 ± 0.02
B	0.18 ± 0.03	0.15 ± 0.04
B LD	0.21 ± 0.05	
Ga + C	0.25 ± 0.06	0.24 ± 0.09
B + C	0.48 ± 0.23	0.30 ± 0.14

The fractions of active gain layer as a function of fluence are shown in Fig. 12 for neutron irradiation and in Fig. 13 for proton irradiation, together with the exponential fits.

Table 4 reports the compilation of measured values of c for neutron (c_n) and proton (c_p) irradiation, and their ratios, ordered in decreasing value. The value of each coefficient has been estimated averaging the measurements of 2 irradiated samples. From the spread of the two measurements, and the uncertainty of the fit, an error of ± 1.0 has been assigned to the determination of c_n while, given the presence of only one measurement per fluence, the error on c_p has been evaluated to be ± 1.5.

For clarity, Table 5 reports the value of the fluence ϕ_o for neutrons and protons. Since the coefficient ϕ_o represents the flux needed to remove 63% of the initial acceptor, Table 5 shows that a carbonated gain layer can withstand more than twice the radiation of a non-carbonated gain layer.

6. Analysis

Several results can be extracted from Table 4 :

- The addition of Carbon improves the radiation resistance: the c_n, c_p coefficients are about a factor of two smaller for B+C and Ga+C LGADs with respect of those of B or Ga. Since no other condition besides the addition of Carbon was changed, we can determine that the presence of Carbon reduces the value of the coefficient k_{cap}.

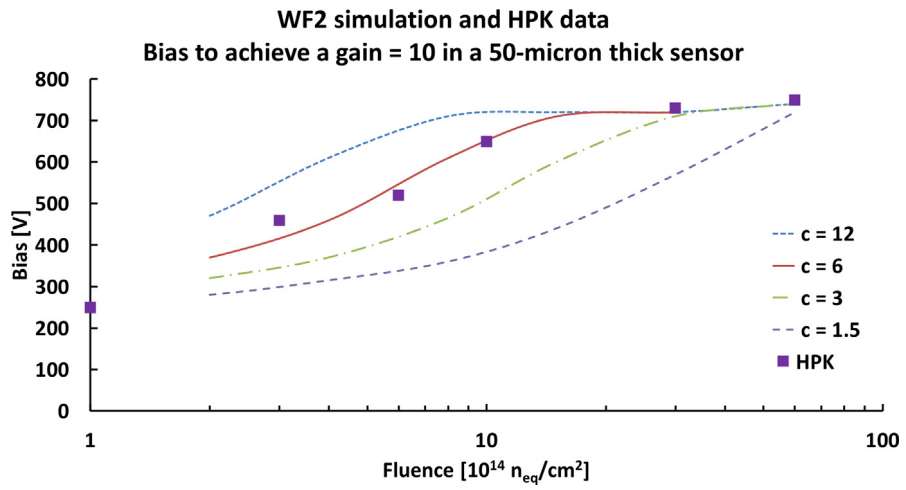

Fig. 10. Evolution of the bias voltage needed to obtain a constant value of gain, G = 10, as a function of fluence: as the gain layer doping is progressively deactivated by irradiation, the bias voltage is increased to compensate for the reduction of the electric field generated by the gain layer. The figure shows how a change in the value of the c exponent (in unit of $[10^{-16}\ \mathrm{cm}^2]$) changes this evolution.

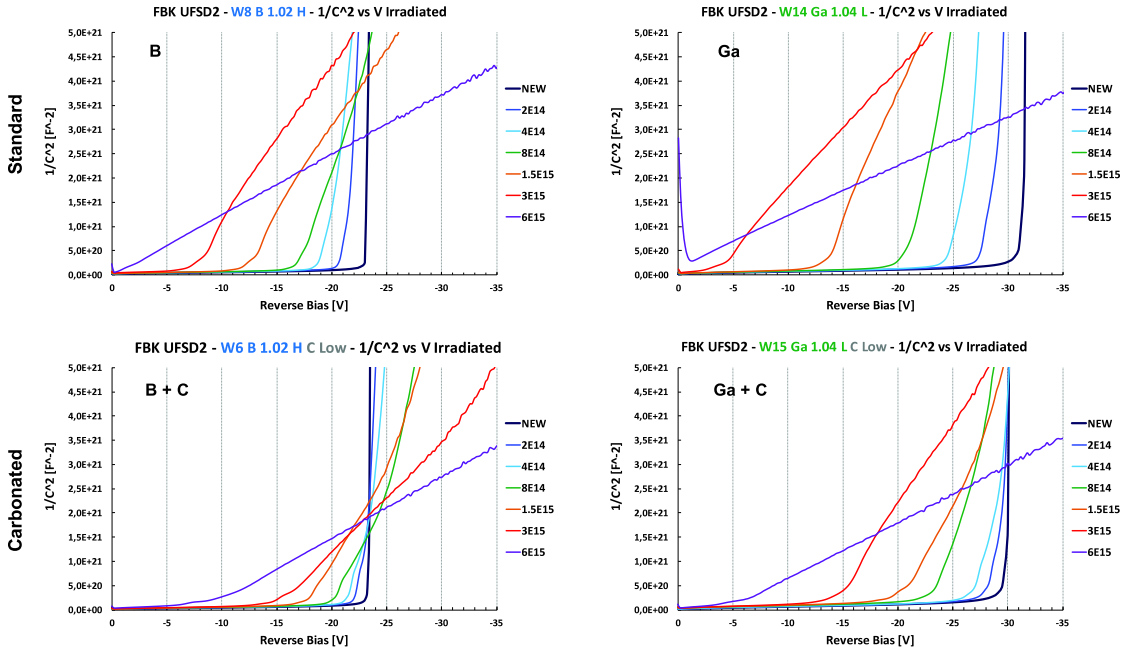

Fig. 11. Evolution of the $1/C^2$-V curve with neutron irradiation for LGAD sensors with different gain layer doping. Irradiation fluence start at $\phi = 2 \cdot 10^{14}\ \mathrm{n_{eq}/cm^2}$ and double at each step up to $\phi = 6 \cdot 10^{15}\ \mathrm{n_{eq}/cm^2}$. Top left: Boron, Top right: Gallium, Bottom left : Boron+Carbon, Bottom right: Gallium+ Carbon.

- Considering the real value of proton fluences, the measured c_p and c_n coefficients are compatible with each other, albeit the c_p values are consistently higher. This effect indicates that the cross section to remove an acceptor, $\sigma_{Acc} = k_{cap} \cdot N_{Int} \cdot \sigma_{Si}$, is similar for a 1 MeV neutron and a 24 GeV/c proton.
- If the NIEL factor is applied to the protons fluence (NIEL = 0.6 for 24 GeV/c protons), the c_p factors are almost twice c_n.
- Narrower and more doped gain layer implants are less prone to initial acceptor removal: B LD has a lower c_n coefficient than B. This is consistent with the expectation from the right pane of Fig. 5 that shows that the relative importance of acceptor removal decreases with increasing initial doping density $\rho_A(0)$.
- The measured coefficients c_p, c_n for Gallium doping are larger than those for Boron doping. This difference is partly due to the lower Gallium density used in W14 with respect of the Boron density in W3 and W8, however, the difference is larger than what it would be just due to this effect. This fact might indicate a higher acceptor removal rate of Gallium doping with respect of that of Boron doping. In [15], a lower acceptor removal rate of Gallium has been measured with respect of the data reported in this work, however, the reason might be that the initial Gallium density in [15] was higher than that of this work.

The gain in LGADs is required to be 20–30: this fact determines that the total amount of doping in the gain layer is roughly a constant in every LGAD. This given amount of doping can be distributed over narrower or wider implants, varying the doping density: equation (6) predicts that in LGADs with wider and less doped implants the initial acceptor removal mechanism is faster. The values of the c_n coefficients as a function of the implant widths reported in Table 2 are shown in

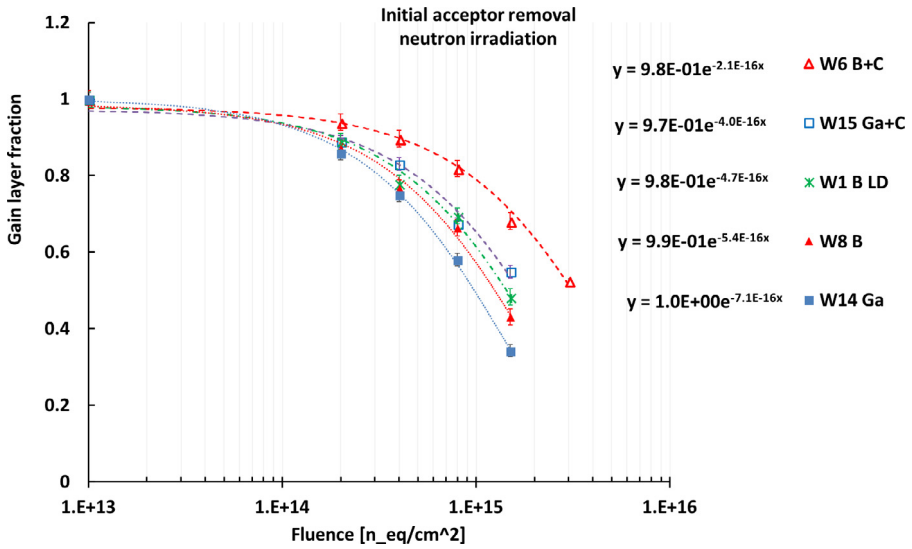

Fig. 12. Fraction of gain layer still active as a function of neutron irradiation.

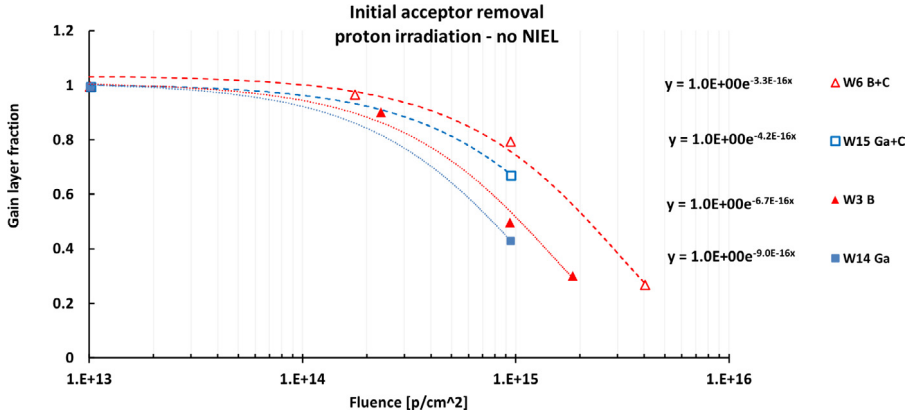

Fig. 13. Fraction of gain layer still active as a function of proton irradiation.

Fig. 14: the plot clearly shows that in wider implants the initial acceptor removal mechanism is faster. This effect holds true also for carbonated gain layers.

A compilation of values of ϕ_o for neutron irradiation measured in this work and in [11–15] is shown in Fig. 15. All sensors are ∼50-μm thick, however, they differ slightly in the doping profile as they do not all have the same gain. The plot reports measurements for LGADs manufactured by CNM with a Gallium or a Boron gain layer, 4 different types of Boron LGADs manufactured by HPK (indicated with the names 50A, 50B, 50C and 50D in order of increasing gain layer doping levels) and several LGADs manufactured by FBK. The carbonated gain layers have clearly the largest values of ϕ_o, followed by B LD: the 1/e fluence for B+C LGADs is almost $0.5 \cdot 10^{16}$ n_{eq}/cm^2.

Fig. 16 updates Fig. 4 including the results obtained in this analysis: the new points cluster around $\rho_A(0) \sim 2 - 6 \cdot 10^{16}$. The value of $\rho_A(0)$ has been obtained by computing the gain layer doping profile using the relationship, shown in Eq. (12), between the derivative of the curve $1/C^2 - V$ and the doping at a depth w.

7. Measurement of the gain due to the gain-layer after a fluence of $\phi = 8 \cdot 10^{14}$, $1.5 \cdot 10^{15}$ and $3 \cdot 10^{15}$ n_{eq}/cm^2.

Using a collimated picosecond laser system with a light spot diameter of ∼ 20 μm and a wavelength of 1064 nm, the gains of B, B LD, B+C, Ga and Ga+C LGADs were measured as a function of bias voltage for 3 neutron irradiation levels: $\phi = 8 \cdot 10^{14}$, $1.5 \cdot 10^{15}$ and $3 \cdot 10^{15}$ n/cm^2. The value of the gain was obtained as the ratio of the signal areas obtained in an LGAD and in a PiN diode irradiated to the same fluence.

The results are shown in Fig. 17: the top left plot shows the gain curves before irradiation, while the following 5 plots show the gain normalized to the respective unirradiated gain at Bias = 150 V. As expected, B+C is the most radiation resistant LGAD: after a fluence of $8 \cdot 10^{14}$ n_{eq}/cm^2 the gain layer still generate at bias = 500 V the same gain as it had when not irradiated at bias = 150 V. Likewise, Ga is the weakest retaining at 500 V only 10% of the initial gain.

Confirming the results on the values of the c_n coefficient, carbonated gain layers (B+C and Ga+C) show higher gain values than those without Carbon for the same fluence level. Likewise, B LD maintains higher gain values than B; at $\phi = 3 \cdot 10^{15}$ n/cm^2 only B+C gain layer is still active. It is possible that by optimizing the Carbon dose this effect can be further enhanced.

8. Conclusions and outlook

50-μm thick LGADs manufactured by FBK with 5 different types of gain layer doping (B, B+C, Ga, Ga+C and B LD) have been irradiated with neutrons and protons. The results show that (i) carbonated gain layer are at least a factor of two more radiation resistant than the equivalent non-carbonated gain layer, (ii) Gallium doping is less radiation resistant than Boron doping, (iii) narrower gain layer implants are more radiation resistant than wider implants, (iv) considering the true fluence value, protons with 24 GeV/c momentum are similarly harmful than

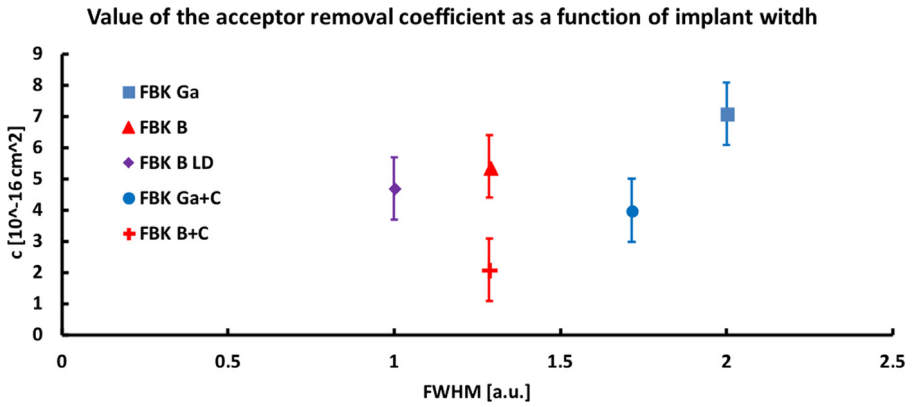

Fig. 14. Initial acceptor removal coefficient c_n as a function of the gain layer implant width for carbonated and non-carbonated gain layers: for wider implants the initial acceptor removal mechanism is faster.

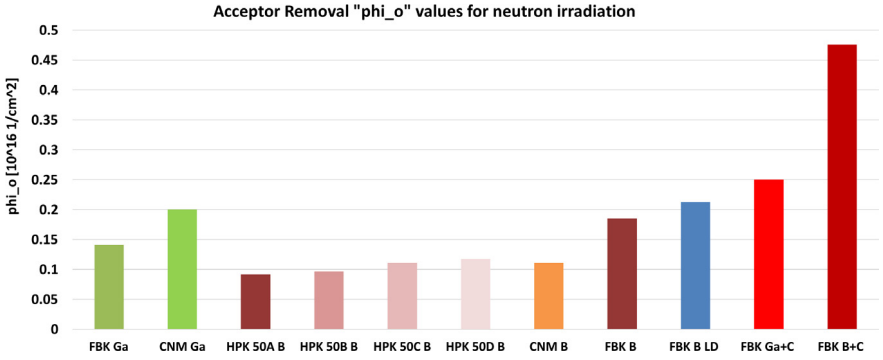

Fig. 15. Compilation of values of the initial acceptor removal coefficient ϕ_o^n for LGADs manufactured by 3 different foundries (HPK, FBK, and CNM) with different gain layer doping compositions.

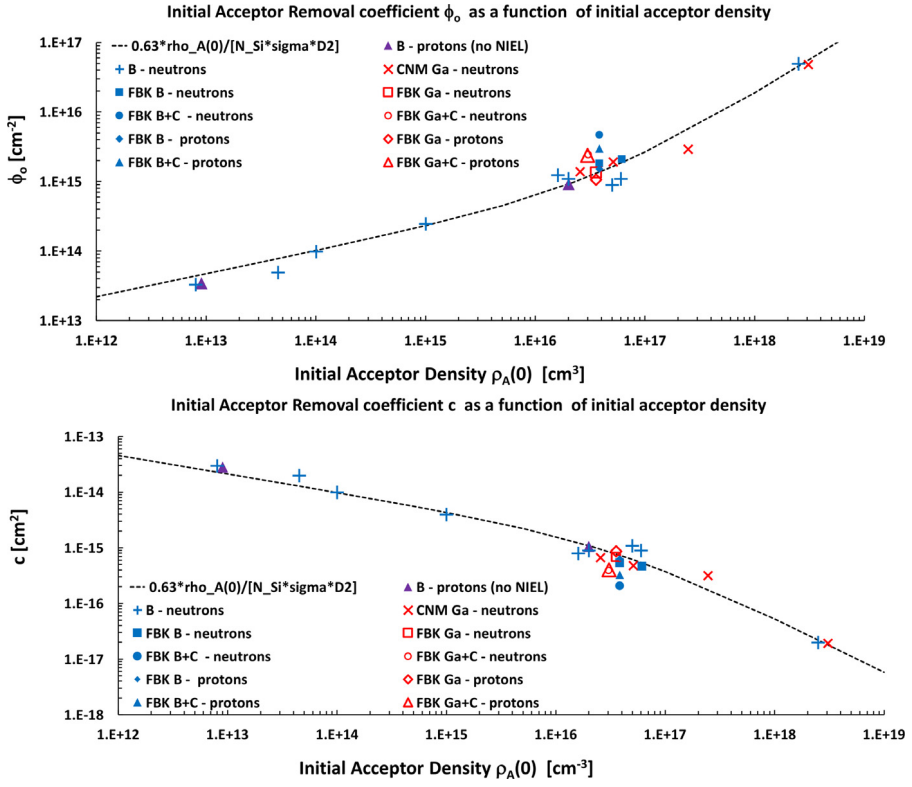

Fig. 16. Values of the ϕ_o and c coefficients from previous measurements and from this analysis.

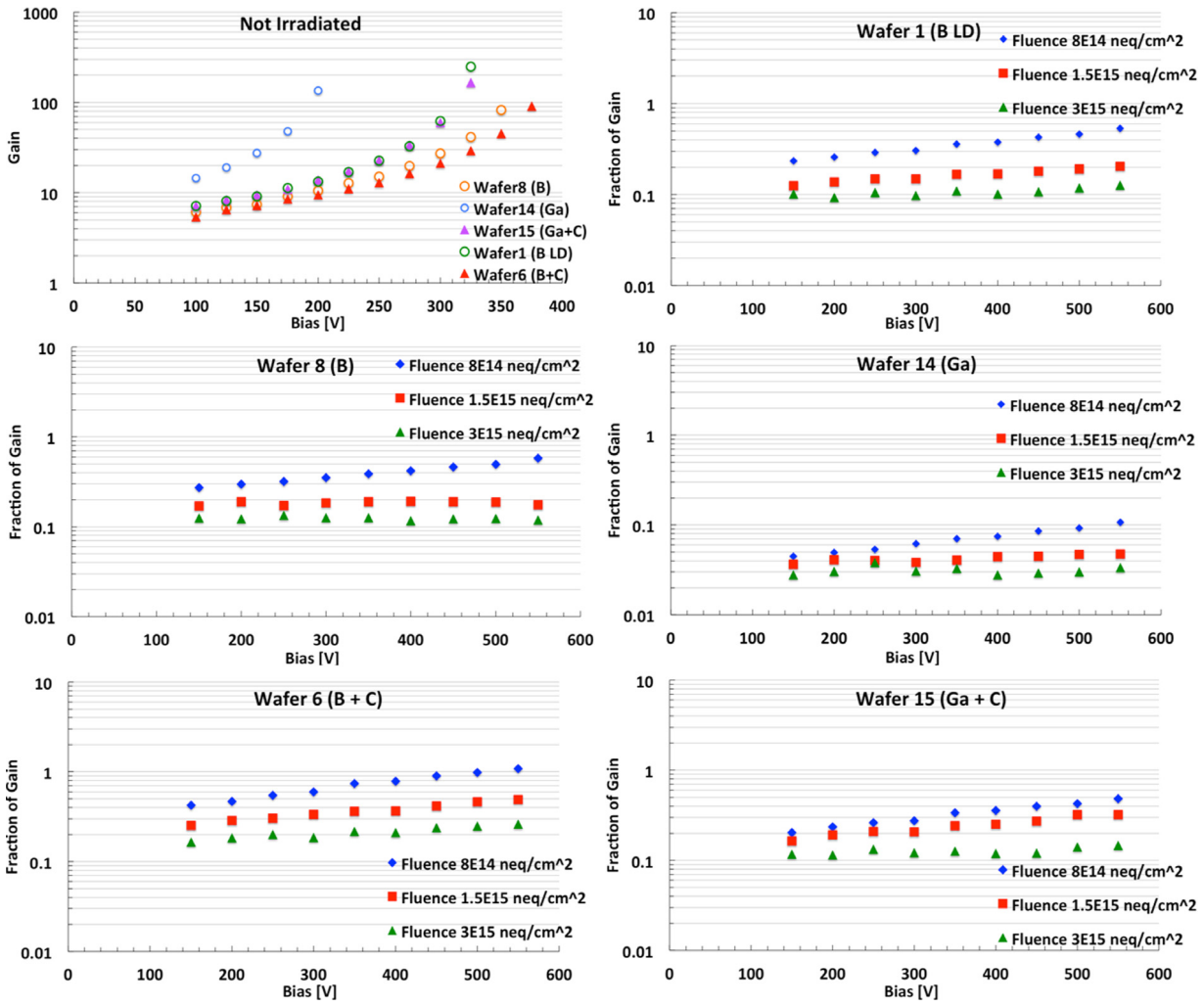

Fig. 17. Top left plot: gain curves before irradiation. Following 5 plots: for each gain layer type, the plot shows the fraction of gain at 3 fluences normalized to each respective gain at Bias = 150 V.

1 MeV neutrons with respect of the initial acceptor removal mechanism, and that (v) if the fluence of protons with 24 GeV/c momentum is converted using the NIEL factor to 1 MeV equivalent neutrons, proton irradiation is much more harmful than that from 1 MeV neutrons .

Carbonated gain layer holds the possibility of designing silicon sensors with gain with enhanced radiation resistance. We plan to further investigate the property of carbonated gain layer by producing gain layers with several carbon doses, to optimize the radiation resistance of the LGAD design. We are confident that these findings, albeit obtained for LGAD sensors, can be successfully implemented in other silicon sensors with gain such as SiPM and APD.

Acknowledgments

We acknowledge the fundamental contributions coming from the discussions, and active collaboration of the RD50 colleagues. We recognize the key contributions of the irradiation facilities at Ljubjiana and IRRAD at CERN. Part of this work has been financed by the European Union's Horizon 2020 Research and Innovation funding program, Italy, under Grant Agreement no. 654168 (AIDA-2020) and Grant Agreement no. 669529 (ERC UFSD669529), and by the Italian Ministero degli Affari Esteri and INFN Gruppo V

References

[1] G. Pellegrini, et al., Technology developments and first measurements of Low Gain Avalanche Detectors (LGAD) for high energy physics applications, Nucl. Instrum. Methods Phys. Res., Sect. A 765 (2014) 12–16.

[2] H.F.-W. Sadrozinski, A. Seiden, N. Cartiglia, 4D tracking with ultra-fast silicon detectors, Rep. Progr. Phys. 81 (2) (2018) 026101, URL http://stacks.iop.org/0034-4885/81/i=2/a=026101.

[3] W. Maes, K. De Meyerm, R. Van Overstraeten, Impact ionization in silicon: A review and update, Solid-State Electron. 33 (1999) 705–718.

[4] G. Kramberger, et al., Radiation effects in Low Gain Avalanche Detectors after hadron irradiations, J. Instrum. 10 (2015) P07006.

[5] Z. Galloway, et al., Properties of HPK UFSD after neutron irradiation up to 6E15 n/cm2 (2017) arXiv:1707.04961.

[6] S. Terada, et al., Proton irradiation on p-bulk silicon strip detectors using 12 GeV PS at KEK, Nucl. Instrum. Methods Phys. Res. A 383 (1) (1996) 159–165, http://dx.doi.org/10.1016/S0168-9002(96)00748-6, URL http://www.sciencedirect.com/science/article/pii/S0168900296007486.

[7] M. Mandurrino, et al., Numerical simulation of charge multiplication in ultra-fast silicon detectors (ufsd) and comparison with experimental data, NSS/MIC IEEE Atlanta. submitted for publication IEEE Nuclear Transaction, 2017, URL https://www.eventclass.org/contxt_ieee2017/download/media?hash=2y13BYBKhVqHCribI5uxmX.JfufYlrAIVzhDJGSQOexR1eteDVyfn8yMK.

[8] J. Balbuena, et al., RD50 Status Report 2008 - Radiation hard semiconductor devices for very high luminosity colliders, CERN-LHCC-2010-012. LHCC-SR-003, CERN, Geneva, URL http://cds.cern.ch/record/1291631.

[9] B. Henderson, Defects and Their Structure in Nonmetallic Solids, in: Nato Science Series B:, Springer US, 2013, URL https://books.google.it/books?id=w3_rBwAAQBAJ.

[10] R. Wunstorf, et al., Investigations of donor and acceptor removal and long term annealing in silicon with different boron/phosphorus ratios, Nucl. Instrum. Methods Phys. Res. A 377 (2) (1996) 228–233, http://dx.doi.org/10.1016/0168-9002(96)00217-3, Proceedings of the Seventh European Symposium on Semiconductor. URL http://www.sciencedirect.com/science/article/pii/0168900296002173.

[11] G. Kramberger, et al., Radiation effects in low gain avalanche detectors after hadron irradiations, J. Instrum. 10 (07) (2015) P07006, URL http://stacks.iop.org/1748-0221/10/i=07/a=P07006.

[12] G. Kramberger, et al., Radiation hardness of thin low gain avalanche detectors, Nucl. Instrum. Methods Phys. Res. A 891 (2018) 68–77, URL http://www.sciencedirect.com/science/article/pii/S0168900218301682.
[13] G. Kramberger, et al., Overview of sensor radiation tolerance at HL-LHC levels, [online], HSTD11, 2017.
[14] M. del Mar Carulla Areste, et al., Last measurements and developments on LGAD detectors, TREDI2017, 2017.
[15] G. Kramberger, et al., Radiation hardness of gallium doped low gain avalanche detectors, Nucl. Instrum. Methods Phys. Res. A 898 (2018) 53–59, http://dx.doi.org/10.1016/j.nima.2018.04.060, URL http://www.sciencedirect.com/science/article/pii/S0168900218305771.
[16] M. Huhtinen, Simulation of non-ionising energy loss and defect formation in silicon, Nucl. Instrum. Methods Phys. Res. A 491 (1) (2002) 194–215, http://dx.doi.org/10.1016/S0168-9002(02)01227-5, URL http://www.sciencedirect.com/science/article/pii/S0168900202012275.
[17] A. Khan, et al., Strategies for improving radiation tolerance of Si space solar cells, Sol. Energy Mater. Sol. Cells 75 (1) (2003) 271–276, http://dx.doi.org/10.1016/S0927-0248(02)00169-1, PVSEC 12 Part II. URL http://www.sciencedirect.com/science/article/pii/S0927024802001691.
[18] G. Paternoster, New developments in Ultra Fast Silicon Detectors at FBK, 31th RD50 Workshop, CERN, Geneva, 2017. URL https://indico.cern.ch/event/663851/contributions/2787294/attachments/1562040/2484362/RD50_17_11_ext.pdf.
[19] Y. Shimizu, et al., Impact of carbon co-implantation on boron distribution and activation in silicon studied by atom probe tomography and spreading resistance measurements, Japan. J. Appl. Phys. 55 (2) (2016) 026501, URL http://stacks.iop.org/1347-4065/55/i=2/a=026501.
[20] L. Snoj, G. Zerovnik, A. Trkov, Computational analysis of irradiation facilities at the JSI TRIGA reactor, Appl. Radiat. Isot. 70 (2012) 483–488.
[21] B. Gkotse, et al., Irradiation Facilities at CERN [online].
[22] F. Cenna, et al., Weightfield2: a fast simulator for silicon and diamond solid state detector, Nucl. Instrum. Methods Phys. Res. A 796 (2015) 149–153, http://dx.doi.org/10.1016/j.nima.2015.04.015, Proceedings of the 10th International Conference on Radiation Effects on Semiconductor Materials Detectors and Devices.